Chapter 4

Mathematical analysis of the magneto-optic scanning microscope

In this chapter the mathematical process for modelling the magneto-optic (MO) scanning microscopes will be described in detail. In the previous chapter diffraction theory was applied to model the response of the Type 1 and confocal reflectance scanning microscopes. A similar approach was applied to modelling the readout process in magneto-optic storage systems by Milster and Curtis [54], where the readout channel is analogous to that of a scanning microscope sensitive to the Kerr effect.

Magneto-optic, MO, imaging, via the Faraday, polar or longitudinal Kerr effects, relies upon the detection of the rotation of the plane of polarisation of a linearly polarised field upon reflection from, or transmission through, a magneto-optic sample. Many detection schemes have been devised which are capable of detecting the very small rotations, typically <1°, introduced by these effects [18,24,55,56]. Alternative detection strategies are also employed to detect the small amount of ellipticity that is introduced upon interaction with a MO sample [57]. However, in the current analysis only detection schemes that are sensitive to the rotation of polarisation are presented. The two most common detection schemes being the single detector [7,24,55,56,58,59] and differential detector [7,27,58,59,60] configurations.

The optical layout of the MO detection schemes are similar to those of the reflectance imaging systems presented in chapter 3. Hence, a similar analysis can be applied to develop a mathematical model of the imaging process in MO systems. The propagation of the electric field through the optical system is formulated using scalar diffraction theory. However, for the MO detection schemes the behaviour and interaction of linearly polarised fields must also be considered. Hence, a Jones matrix

analysis will be employed to describe the interaction of the polarised field with the MO sample and the optics of the readout channel [27,60,61,62,63].

The Type 1 configuration of the differential detector MO scanning microscope is commonly employed as the readout head in optical storage systems [7,60,64,65] and will be analysed in detail in the current chapter. However, it is interesting, for completeness, to develop an expression describing the imaging process in the alternative single detector arrangement.

A magneto-optic confocal arrangement is also often employed by researchers to image magnetic thin films [10,11,12,13,14,48,49,66], and so will also be analysed here in detail.

4.1 The single detector MO scanning microscope

The single detector MO system relies on the use of an analyser in conjunction with single photo-detector to generate a signal which is proportional to the rotation of polarisation of the linearly polarised field after interaction with an MO sample.

4.1.1 The Type 1 system

Illustrated in Fig. 4.1 is the optical layout of the simplest MO detection scheme, that of the Type 1 single detector MO scanning microscope [7,24,55,56,58,59].

Optical configuration

The illumination is provided by a linearly polarised coherent source, such as a laser, that is focused onto the surface of the sample by the objective lens. A polariser in the illumination path is often used to enhance the incident polarisation state. After interaction with the sample an orthogonal *y* component of polarisation is introduced into the transmitted field by the magneto-optic effect, along with any phase variations introduced by the sample. The transmitted field then propagates to the collector lens by the diffraction process, where it is collimated and propagates to the analyser. The

analyser is aligned so that its transmission axis is at an angle $b°$ to the plane of incident polarisation and acts to transmit the field component that is polarised along its transmission axis. Hence, the field components are resolved along the axis of the analyser and then propagate, without further modification, to a large area photo-detector, here assumed to have uniform responsivity. Although Fig. 4.1 illustrates the optical system operating in transmission, it is common to employ the MO detection system in reflection [18,59], in which case a beamsplitter is placed prior to the objective lens to separate incident and reflected fields.

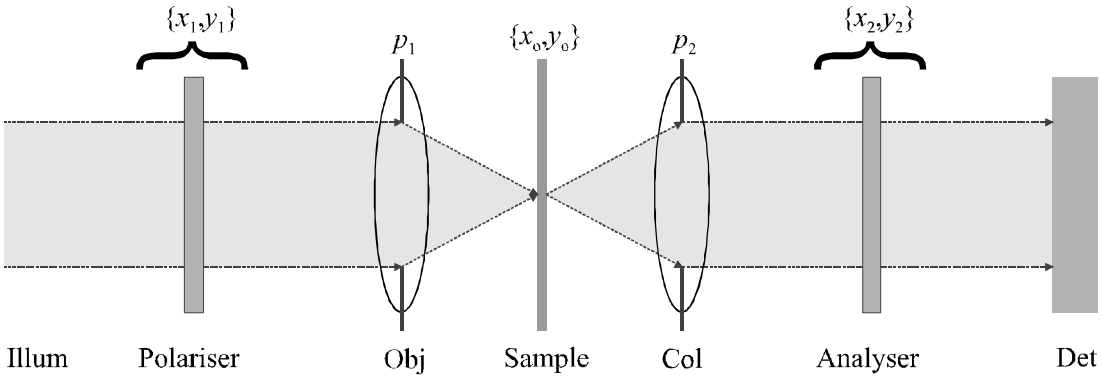

Figure 4.1 : *The optical layout of the single detector MO scanning microscope.*

Image calculation

Assuming a uniform incident field distribution, $y_x(x_1, y_1)$, that is linearly polarised in *x*, then the field distribution, $y_x(x_o, y_o)$, at the surface of the sample (the focal point of the objective lens) is as calculated previously in sec 2.5 and chapter 3, and is given by

$$y_x(x_o, y_o) = \mathrm{FT}\{p_1(x_1, y_1) y_x(x_1, y_1)\} = h_1(x_o, y_o) \tag{4.1}$$

where $p_1(x_1, y_1)$ is the objective aperture pupil function and $h_1(x_o, y_o)$ is the amplitude point spread function of the objective lens. The interaction of the incident field distribution, $y_x(x_o, y_o)$, and the MO properties of the sample can be represented by the Jones matrix characteristic [56,61]

$$\begin{bmatrix} y_x' \\ y_y' \end{bmatrix} = r_x \cdot \begin{bmatrix} 1 & \pm\tan(a)\exp(-jf) \\ \pm\tan(a)\exp(-jf) & -1 \end{bmatrix} \cdot \begin{bmatrix} y_x \\ 0 \end{bmatrix} \tag{4.2}$$

where y_x' and y_y' are the orthogonal polarised field components after reflection from, or transmission through, the MO sample, r_x represents the complex amplitude reflectance of the sample, tan(a) represents the tangent of Kerr rotation, and f represents the phase difference between the x and y polarised field components. The introduction of an orthogonal y component of polarisation can be viewed as the rotation of the plane of polarisation after reflection from, or transmission through, the MO sample and the phase difference contributes to ellipticity in the readout beam. Hence, after interaction with the MO sample the reflected field distribution is composed of orthogonal x and y polarised field components given by

$$\begin{aligned} y_x'(x_o, y_o) &= h_1(x_o, y_o) r_x(x_o - x_s, y_o - y_s) \\ y_y'(x_o, y_o) &= h_1(x_o, y_o) r_x(x_o - x_s, y_o - y_s) \tan\big(a(x_o - x_s, y_o - y_s)\big) \\ &\quad \cdot \exp\{-jf(x_o - x_s, y_o - y_s)\} \end{aligned} \tag{4.3}$$

where (x_s, y_s) is the scan position on the sample and all other symbols have their usual meaning. The orthogonal field components, $y_x(x_2, y_2)$ and $y_y(x_2, y_2)$, in the plane of the collector lens are given by the two-dimensional Fourier transform of the field components, $y_x'(x_o, y_o)$ and $y_y'(x_o, y_o)$, immediately after interaction with the MO sample, i.e.

$$\begin{aligned} y_x(x_2, y_2) &= \frac{1}{l f} \iint_{-\infty}^{\infty} y_x'(x_o, y_o) \exp\left\{\frac{jk}{f}(x_2 x_o + y_2 y_o)\right\} dx_o dy_o \\ y_y(x_2, y_2) &= \frac{1}{l f} \iint_{-\infty}^{\infty} y_y'(x_o, y_o) \exp\left\{\frac{jk}{f}(x_2 x_o + y_2 y_o)\right\} dx_o dy_o \end{aligned} \tag{4.4}$$

where f is the focal length of the collector lens (which is assumed to be equal to the focal length of the objective lens). Immediately after the collector lens the orthogonal field components, $y_x(x_2, y_2)$ and $y_y(x_2, y_2)$, are modified by the aperture pupil function of the collector lens to give,

$$\begin{aligned} y_x'(x_2, y_2) &= y_x(x_2, y_2) p_2(x_2, y_2) \\ y_y'(x_2, y_2) &= y_y(x_2, y_2) p_2(x_2, y_2) \end{aligned} \tag{4.5}$$

where $p_2(x_2, y_2)$ is the collector aperture pupil function.

If the transmission axis of the analyser is aligned at an angle $b°$ to the plane of incident polarisation, x, then upon propagation through the analyser the orthogonal

field components, $y_x'(x_2, y_2)$ and $y_y'(x_2, y_2)$, will be resolved along the transmission axis of the analyser to give

$$y''(x_2, y_2) = y_x'(x_2, y_2)\cos b + y_y'(x_2, y_2)\sin b \quad . \tag{4.6}$$

The field then propagates, without further modification, to the large area photo-detector, which is assumed to be of uniform responsivity and equal to unity. The signal from the photo-detector is as calculated previously, and is given by the integral, over the area of the photo-detector, of the square magnitude of the incident field distribution, i.e.

$$I(x_s, y_s) = \iint_{-\infty}^{\infty} \left| y''(x_2, y_2) \right|^2 dx_2 dy_2 \tag{4.7}$$

which substituting for $y''(x_2, y_2)$ from eq. (4.6) gives

$$I(x_s, y_s) = \iint_{-\infty}^{\infty} \left| y_x'(x_2, y_2)\cos b + y_y'(x_2, y_2)\sin b \right|^2 dx_2 dy_2 \ . \tag{4.8}$$

Substituting for $y_x'(x_2, y_2)$ and $y_y'(x_2, y_2)$ from eq. (4.5) and rearranging gives

$$\begin{aligned} I(x_s, y_s) = \iint_{-\infty}^{\infty} \left| p_2(x_2, y_2) \right|^2 & \left(y_x(x_2, y_2)\cos b + y_y(x_2, y_2)\sin b \right) \\ & \cdot \left(y_x(x_2, y_2)\cos b + y_y(x_2, y_2)\sin b \right)^* dx_2 dy_2 \end{aligned} \tag{4.9}$$

where * represents complex conjugation. Substituting for $y_x(x_2, y_2)$ and $y_y(x_2, y_2)$ from eq. (4.4) gives

$$\begin{aligned} I(x_s, y_s) = & \iint_{-\infty}^{\infty} \left| p_2(x_2, y_2) \right|^2 \\ & \cdot \left(\frac{1}{lf} \iint_{-\infty}^{\infty} \left(y_x'(x_o, y_o)\cos b + y_y'(x_o, y_o)\sin b \right) \exp\left\{ \frac{jk}{f}(x_2 x_o + y_2 y_o) \right\} dx_o' dy_o' \right) \\ & \cdot \left(\frac{1}{lf} \iint_{-\infty}^{\infty} \left(y_x'^*(x_o', y_o')\cos b + y_y'^*(x_o', y_o')\sin b \right) \exp\left\{ \frac{-jk}{f}(x_2 x_o' + y_2 y_o') \right\} dx_o' dy_o' \right) \\ & dx_2 dy_2 \end{aligned} \tag{4.10}$$

where x_o' and y_o' are dummy variables. Rearranging eq. (4.10) and substituting for $y_x'(x_o, y_o)$ and $y_y'(x_o, y_o)$ from eq. (4.3) gives

$$I(x_s, y_s) = \iiint_{-\infty}^{\infty} g_2(x_o - x_o', y_o - y_o') h_1(x_o, y_o) h_1^*(x_o', y_o')$$
$$\left(r_x(x_o - x_s, y_o - y_s)\cos b + r_x(x_o - x_s, y_o - y_s)\tan\left(a(x_o - x_s, y_o - y_s)\right)\exp\left(-jf(x_o - x_s, y_o - y_s)\right)\sin b\right)$$
$$\left(r_x^*(x_o' - x_s, y_o' - y_s)\cos b + r_x^*(x_o' - x_s, y_o' - y_s)\left[\tan\left(a(x_o' - x_s, y_o' - y_s)\right)^*\right]\exp\left(jf(x_o' - x_s, y_o' - y_s)\right)\sin b\right)$$
$$dx_o dy_o dx_o' dy_o' \qquad (4.11)$$

where constant scaling factors have been ignored and $g_2(x_o, y_o)$ is the amplitude point spread function associated with the square magnitude of the collector aperture pupil function, as given by eq. (3.11).

To maximise the signal from the Type 1 single detector MO scanning microscope the analyser must be aligned so that only the MO signal propagates to the photo-detector, i.e. only the *y* component of the reflected field generated after interaction with the MO sample. Hence, by setting b = 90° the signal from the photo-detector will be sensitive to only the MO properties of the sample, and the resultant signal from the Type 1 single detector MO scanning microscope is given by

$$\begin{aligned} I(x_s, y_s) = \iiint_{-\infty}^{\infty} & g_2(x_o - x_o', y_o - y_o') \\ & \cdot h_1(x_o, y_o) r_x(x_o - x_s, y_o - y_s) h_1^*(x_o', y_o') r_x^*(x_o' - x_s, y_o' - y_s) \\ & \cdot \tan\left(a(x_o - x_s, y_o - y_s)\right)\exp\left(-jf(x_o - x_s, y_o - y_s)\right) \\ & \cdot \left[\tan\left(a(x_o' - x_s, y_o' - y_s)\right)^*\right]\exp\left(jf(x_o' - x_s, y_o' - y_s)\right) dx_o dy_o dx_o' dy_o' \end{aligned} \qquad . \quad (4.12)$$

Transfer function representation

A transfer function representation of the signal generated in the Type 1 single detector MO scanning microscope can be obtained using a similar analysis as developed for generating the transfer function model for the ordinary reflectance scanning microscope, described in sec. 3.2 and sec. 3.3.

If the reflectance and MO properties of the sample are expressed in terms of their associated spectra, $\Gamma(n_x,n_y)$ and $\Lambda(n_x,n_y)$ respectively, i.e.

$$r_x(x,y) = \iint_{-\infty}^{\infty} \Gamma(n_x,n_y)\exp\{-2pj(n_x x + n_y y)\}\,dn_x dn_y$$

$$\left[r_x(x,y)\tan(a(x,y))\exp\{-jf(x,y)\}\right] = \iint_{-\infty}^{\infty} \Lambda(n_x,n_y)\exp\{-2pj(n_x x + n_y y)\}\,dn_x dn_y \tag{4.13}$$

where n_x and n_y are orthogonal spatial frequency components, then substituting into eq. (4.11), gives

$$\begin{aligned} I(x_s,y_s) = \iint\iint_{-\infty}^{\infty} \Big[& \iint\iint_{-\infty}^{\infty} h_1(x_o,y_o)h_1{}^*(x_o',y_o')g_2(x_o-x_o',y_o-y_o') \\ & \cdot\exp\{-2pj(n_y x_o + n_y x_o)\}\exp\{2pj(n_y' x_o' + n_y' x_o')\}dx_o dy_o dx_o' dy_o' \Big] \\ & \cdot\left(\Gamma(n_x,n_y)\cos b + \Lambda(n_x,n_y)\sin b\right)\left(\Gamma^*(n_x',n_y')\cos b + \Lambda^*(n_x',n_y')\sin b\right) \\ & \cdot\exp\{2pj((n_x-n_x')x_s + (n_y-n_y')y_s)\}dn_x dn_y dn_x' dn_y' \end{aligned} \tag{4.14}$$

Comparing eq. (4.14) and eq. (3.31) it can be seen that the integral in the square brackets of eq. (4.14) represents the Type 1 PCTF. Hence, the signal from the Type 1 single detector MO scanning microscope can be expressed in the characteristic form of eq. (3.32), i.e.

$$\begin{aligned} I(x_s,y_s) = \iint\iint_{-\infty}^{\infty} & C(n_x,n_y;n_x',n_y')M(n_x,n_y;n_x',n_y') \\ & \cdot\exp\{2p\,j[(n_x-n_x')x_s + (n_y-n_y')y_s]\}\;dn_x\,dn_y\,dn_x'\,dn_y' \end{aligned} \tag{3.32}$$

where the medium function, $M(n_x,n_y;n_x',n_y')$, is now a function of the reflectance and the MO properties of the sample, and the rotation of the transmission axis of the analyser. Comparing eq. (3.32) and eq. (4.14) it can be seen that the medium function for the single detector MO system can be expressed in the form

$$\begin{aligned} M(n_x,n_y;n_x',n_y') = & \left(\Gamma^*(n_x',n_y')\cos b + \Lambda^*(n_x',n_y')\sin b\right) \\ & \cdot\left(\Gamma(n_x,n_y)\cos b + \Lambda(n_x,n_y)\sin b\right) \end{aligned} \tag{4.15}$$

If the analyser is aligned so as to maximise the Kerr signal, i.e. b=90°, then eq. (4.15) reduces to the form

$$M\left(n_x, n_y; n_x', n_y'\right) = \Lambda\left(n_x, n_y\right)\Lambda^*\left(n_x', n_y'\right) \tag{4.16}$$

and it can be seen that, as expected, the signal from the photo-detector is sensitive only to the MO properties of the sample, i.e. detects only the magneto-optically induced *y* component of polarisation.

If the analyser is aligned to the same direction as the incident polarisation, i.e. *x*, then it can be seen that the medium function reduces to the same form as for the Type 1 reflectance scanning microscope, as given by eq. (3.33), and the system no longer images magneto-optic contrast.

The response of the Type 1 single detector MO scanning microscope can now be modelled in computer code using the 'direct calculation' approach for simple one-dimensional and two-dimensional MO objects, which is described in sec. 5.2, and the 'transfer function' approach for simple one-dimensional objects, which is described in sec. 6.3.1.

4.1.2 The confocal system

It is the aim of this section to describe the signal generation process in the confocal configuration of the single detector MO scanning microscope.

Optical configuration

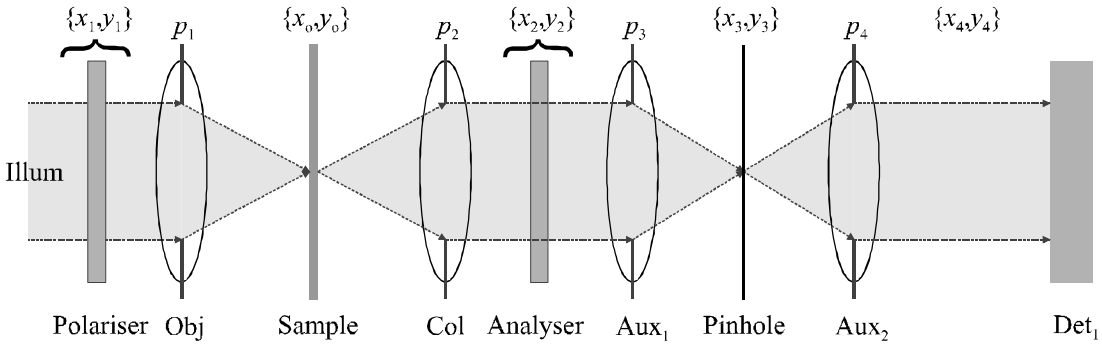

Figure 4.2 : *The optical layout of the confocal single detector MO scanning microscope.*

Figure 4.2. illustrates the optical layout of the confocal single detector MO scanning microscope which is similar to that of the Type 1 single detector MO scanning microscope illustrated in Fig. 4.1, where the confocal arrangement is implemented by the introduction of a pinhole aperture and auxiliary lens arrangement into the detection arm.

Image calculation

The field distribution in the plane of auxiliary lens 1 is equal to the field distribution incident on the photo-detector in the Type 1 configuration, as given previously by eq. (4.6), assuming the incident illumination is linearly polarised in *x*.

The field distribution, $y'''(x_2, y_2)$, immediately after auxiliary lens 1 is given by

$$\begin{aligned} y'''(x_2, y_2) &= y''(x_2, y_2)\, p_3(x_2, y_2) \\ &= p_3(x_2, y_2)\, p_2(x_2, y_2)\left(y_x(x_2, y_2)\cos b + y_y(x_2, y_2)\sin b\right) \end{aligned} \tag{4.17}$$

where $p_3(x_2, y_2)$ is the aperture pupil function of auxiliary lens 1, $p_2(x_2, y_2)$ is the collector aperture pupil function, and $y_x(x_2, y_2)$ and $y_y(x_2, y_2)$ are the orthogonal field components immediately before transmission through the analyser. The field distribution, $y(x_3, y_3)$, in the plane of the confocal pinhole is given by the two-dimensional Fourier transform of the field distribution, $y'''(x_2, y_2)$, immediately after the auxiliary lens 1, i.e.

$$y(x_3, y_3) = \frac{1}{l f_{A1}} \iint_{-\infty}^{\infty} y'''(x_2, y_2) \exp\left\{\frac{jk}{f_{A1}}(x_3 x_2 + y_3 y_2)\right\} dx_2 dy_2 \tag{4.18}$$

where f_{A1} is the focal length of auxiliary lens 1, and all other symbols have their usual meaning. Immediately after the pinhole aperture the field distribution is modified by the aperture function of the pinhole, $p_p(x_3, y_3)$, to give

$$y'(x_3, y_3) = y(x_3, y_3)\, p_p(x_3, y_3) \quad . \tag{4.19}$$

The field distribution, $y(x_4, y_4)$, in the plane of auxiliary lens 2 is given by the two-dimensional Fourier transform of the field distribution, $y'(x_3, y_3)$, immediately after the pinhole aperture, i.e.

$$y\left(x_4, y_4\right) = \frac{1}{l f_{A2}} \iint_{-\infty}^{\infty} y'\left(x_3, y_3\right) \exp\left\{ \frac{jk}{f_{A2}} \left(x_4 x_3 + y_4 y_3\right) \right\} dx_3 dy_3 \qquad (4.20)$$

where f_{A2} is the focal length of auxiliary lens 2 and all other symbols have their usual meaning. The field distribution is then modified by the aperture pupil function of auxiliary lens 2, $p_4(x_4, y_4)$, to give

$$y'\left(x_4, y_4\right) = y\left(x_4, y_4\right) p_4\left(x_4, y_4\right) \quad . \qquad (4.21)$$

The field then propagates, without further modification, towards the large area photo-detector, which is assumed to be of uniform responsivity and equal to unity. The signal from the photo-detector is calculated as previously, and is given by the integral, over the area of the photo-detector, of the square magnitude of the incident field distribution, i.e.

$$I\left(x_s, y_s\right) = \iint_{-\infty}^{\infty} \left| y'\left(x_4, y_4\right) \right|^2 dx_4 dy_4 \qquad (4.22)$$

which by substituting for $y'(x_4, y_4)$ from eq. (4.21) and rearranging gives

$$I\left(x_s, y_s\right) = \iint_{-\infty}^{\infty} \left| p_4\left(x_4, y_4\right) \right|^2 y\left(x_4, y_4\right) y^*\left(x_4, y_4\right) dx_4 dy_4 \quad . \qquad (4.23)$$

If it assumed that auxiliary lens 2 collects all the light emanating from the pinhole aperture, then $p_4(x_4, y_4)$ can be seen to be assumed to be equal to unity and eq. (4.23) can be written, using Rayleigh's theorem, as

$$I\left(x_s, y_s\right) = \iint_{-\infty}^{\infty} \left| p_p\left(x_3, y_3\right) \right|^2 y\left(x_3, y_3\right) y^*\left(x_3, y_3\right) dx_3 dy_3 \quad . \qquad (4.24)$$

Substituting for $y(x_3, y_3)$ from eq. (4.18) and rearranging gives

$$I\left(x_s, y_s\right) = \iint_{-\infty}^{\infty} \iint_{-\infty}^{\infty} \left[\iint_{-\infty}^{\infty} \left| p_p\left(x_3, y_3\right) \right|^2 \exp\left\{ \frac{jk}{f_{A1}} \left(x_3\left(x_2 - x_2'\right) + y_3\left(y_2 - y_2'\right) \right) \right\} dx_3 dy_3 \right] \cdot y'''\left(x_2, y_2\right) y'''^*\left(x_2', y_2'\right) dx_2 dy_2 dx_2' dy_2' \qquad (4.25)$$

which simplifies to give

$$I\left(x_s, y_s\right) = \iint_{-\infty}^{\infty} \iint_{-\infty}^{\infty} G\left(x_2 - x_2', y_2 - y_2'\right) y'''\left(x_2, y_2\right) y'''^*\left(x_2', y_2'\right) dx_2 dy_2 dx_2' dy_2' \qquad (4.26)$$

where constant scaling factors have been ignored and $G(x_2, y_2)$ is the Fourier transform of the square magnitude of the pinhole aperture pupil function as given by eq. (3.62). Substituting for $y'''(x_2, y_2)$ from eq. (4.17) into eq. (4.26) yields

$$I(x_s, y_s) = \int_{-\infty}^{\infty}\int_{-\infty}^{\infty} G(x_2 - x_2', y_2 - y_2')\, p_c(x_2, y_2)\, p_c{}^*(x_2', y_2') \cdot \left(y_x(x_2, y_2)\cos b + y_y(x_2, y_2)\sin b\right)\left(y_x{}^*(x_2', y_2')\cos b + y_y{}^*(x_2', y_2')\sin b\right) \cdot dx_2\, dy_2\, dx_2'\, dy_2' \tag{4.27}$$

where $p_c(x_2, y_2)$ is the combined aperture pupil function of the collector and auxiliary lenses as given by eq. (3.46). Substituting for $y_x(x_2, y_2)$ and $y_y(x_2, y_2)$ from eq. (4.4) and rearranging gives

$$I(x_s, y_s) = \int_{-\infty}^{\infty}\int_{-\infty}^{\infty} \left[\int_{-\infty}^{\infty}\int_{-\infty}^{\infty} G(x_2 - x_2', y_2 - y_2')\, p_c(x_2, y_2)\, p_c{}^*(x_2', y_2') \cdot \exp\left\{\frac{jk}{f}(x_2 x_o + y_2 y_o)\right\}\exp\left\{\frac{-jk}{f}(x_2' x_o' + y_2' y_o')\right\} dx_2\, dy_2\, dx_2'\, dy_2'\right] \cdot \left(y_x'(x_o, y_o)\cos b + y_y'(x_o, y_o)\sin b\right) \left(y_x'{}^*(x_o', y_o')\cos b + y_y'{}^*(x_o', y_o')\sin b\right) \cdot dx_o\, dy_o\, dx_o'\, dy_o' \tag{4.28}$$

which simplifies to

$$I(x_s, y_s) = \int_{-\infty}^{\infty}\int_{-\infty}^{\infty} g(x_o, y_o; x_o', y_o')\left(y_x'(x_o, y_o)\cos b + y_y'(x_o, y_o)\sin b\right) \cdot \left(y_x'{}^*(x_o', y_o')\cos b + y_y'{}^*(x_o', y_o')\sin b\right) dx_o\, dy_o\, dx_o'\, dy_o' \tag{4.29}$$

where $g(x_o, y_o; x_o', y_o')$ is as given by eq. (3.49). Substituting for $y_x'(x_o, y_o)$ and $y_y'(x_o, y_o)$ from eq. (4.3) and rearranging yields

$$I(x_s,y_s)=\iint_{-\infty}^{\infty}\iint g_2(x_o,y_o;x_o',y_o')h_1(x_o,y_o)h_1*(x_o',y_o')$$
$$\left(r_x(x_o-x_s,y_o-y_s)\cos b+r_x(x_o-x_s,y_o-y_s)\tan\left(a(x_o-x_s,y_o-y_s)\right)\exp\left(-jf(x_o-x_s,y_o-y_s)\right)\sin b\right)$$
$$\left(r_x*(x_o'-x_s,y_o'-y_s)\cos b+r_x*(x_o'-x_s,y_o'-y_s)\tan\left(a(x_o'-x_s,y_o'-y_s)\right)*\exp\left(jf(x_o'-x_s,y_o'-y_s)\right)\sin b\right)$$
$$dx_o dy_o dx_o' dy_o' \tag{4.30}$$

It can be seen that the signal from the confocal single detector arrangement is similar to that obtained in the Type 1 single detector MO scanning microscope as illustrated in eq. (4.11). However, for the confocal configuration the signal depends upon the function $g(x_o,y_o;x_o',y_o')$ that is a function of the Fourier transform of the square magnitude of the pinhole aperture pupil function. A similar result was obtained when comparing the expressions representing the signals generated in the Type 1 and the confocal reflectance scanning microscopes, eq. (3.10) and eq. (3.64) respectively.

Transfer function representation

A transfer function representation of the signal from the confocal single detector MO can be generated following that analysis presented for the Type 1 single detector MO system, sec. 4.1.1.

Expressing the reflectance and MO properties of the sample in terms of their associated spectra, $\Gamma(n_x,n_y)$ and $\Lambda(n_x,n_y)$ respectively, as given by eq. (4.13), and substituting into eq. (4.30) gives

$$\begin{aligned}I(x_s,y_s)=\iint_{-\infty}^{\infty}\iint\Bigg[&\iint_{-\infty}^{\infty}\iint h_1(x_o,y_o)h_1*(x_o',y_o')g_2(x_o,y_o;x_o',y_o')\\&\cdot\exp\left\{-2pj\left(n_y x_o+n_y x_o\right)\right\}\exp\left\{2pj\left(n_y' x_o'+n_y' x_o'\right)\right\}dx_o dy_o dx_o' dy_o'\Bigg]\\&\cdot\left(\Gamma(n_x,n_y)\cos b+\Lambda(n_x,n_y)\sin b\right)\left(\Gamma*(n_x',n_y')\cos b+\Lambda*(n_x',n_y')\sin b\right)\\&\cdot\exp\left\{2pj\left((n_x-n_x')x_s+(n_y-n_y')y_s\right)\right\}dn_x dn_y dn_x' dn_y'\end{aligned} \tag{4.31}$$

where all symbols have their usual meaning.

Comparing eq. (4.31) with eq. (4.14) it can again be seen that the only difference is the dependence on the pinhole pupil function explicit in the function $g_2(x_o, y_o; x_o', y_o')$ for the confocal case. The signal from the confocal single detector MO scanning microscope can also be expressed in the characteristic form of eq. (3.32) with a medium function defined by eq. (4.15) and a confocal PCTF as given by eq. (3.73).

In sec. 6.3.2 the transfer function approach will be used to model the response of the confocal single detector MO scanning microscope for simple one-dimensional MO objects.

4.2 The differential detector MO scanning microscope

It has already been mentioned that the optical configuration of the differential detector MO scanning microscope is commonly used in the readout head of optical storage systems. The differential detector MO system relies upon a differential detection configuration to produce a signal which is proportional to the rotation of the plane of polarisation, the polarity of the signal determining the direction of the rotation of polarisation. An advantage of the differential detector configuration is that it helps to reduce common mode signals and so offers improved signal to noise ratio over the single detector MO system [7,58,59,60].

4.2.1 The Type 1 system

Figure 4.3 illustrates the optical channel of the Type 1 differential detector MO scanning microscope. The differential detector arrangement, consisting of a half wave plate and polarising beamsplitter placed after the collector aperture, ensures that equal but opposite signals are generated at the two photo-detectors. The signals are fed through a differential amplifier arrangement such that the difference signal is generated.

Optical configuration

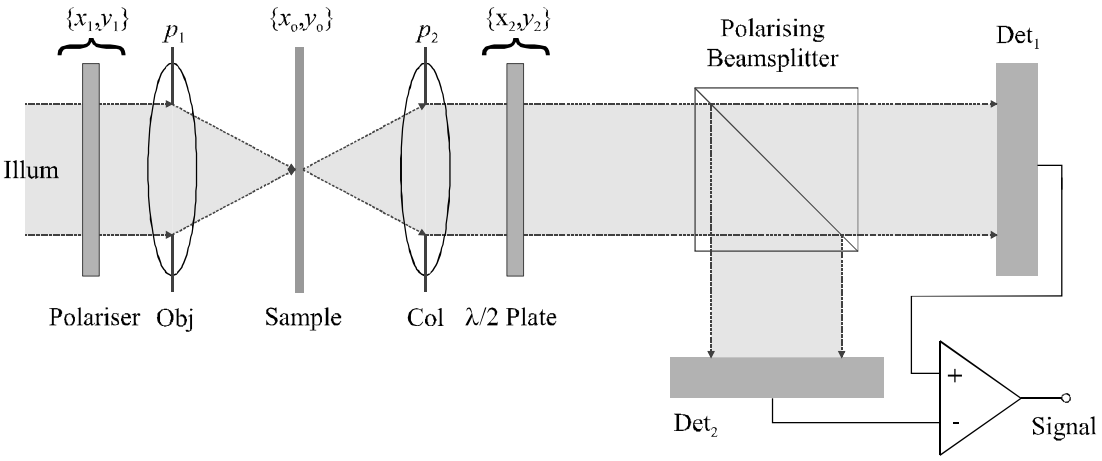

Figure 4.3 : *The optical layout of the Type 1 differential detector MO scanning microscope.*

The propagation of the orthogonal field distributions to the plane of the half wave plate are as described for the single detector MO configuration to the plane of the analyser. The half wave plate acts so as to balance the signals on the two photo-detectors [65], thus removing common mode signals. The half wave plate rotates the plane of polarisation of linearly polarised incident light by an amount which is twice that angle subtended between the principle axis of the half wave plate and the angle of the incident linearly polarised field. The modified field components then propagate towards to the differential detection arm of the instrument. The polarising beamsplitter acts such that the *x* component propagates through the polarising beamsplitter towards photo-detector 1, and the *y* component is reflected at the interface of the polarising beamsplitter towards photo-detector 2. The signal is then generated by calculating the difference signal between the two signals from the photo-detectors. In normal operation the half wave plate and polarising beamsplitter arrangement are aligned such that in the absence of the Kerr effect each photo-detector will receive equal amounts of light and the difference signal will be zero. However, in the presence of a Kerr rotation the photo-detectors will receive unequal amounts of light and a difference signal will be generated at the output of the differential amplifier. Although Fig. 4.3 illustrates the optical system operating in

transmission it is common to operate the differential detector MO system in reflectance [18,59], in which case a beamsplitter is placed prior to the objective lens to separate incident and reflected fields.

Image calculation

The orthogonal field components immediately after the plane of the collector lens are as calculated for the single detector MO scanning microscope, given by eq. (4.5), for an incident illumination, which is linearly polarised in *x*.

The effects of the half wave plate can be described using the Jones matrix [27,54]

$$\begin{bmatrix} y_x'' \\ y_y'' \end{bmatrix} = \begin{bmatrix} \cos 2q & \sin 2q \\ -\sin 2q & \cos 2q \end{bmatrix} \cdot \begin{bmatrix} y_x' \\ y_y' \end{bmatrix} \tag{4.32}$$

where y_x' and y_y' are the orthogonal field components immediately before the half wave plate, y_x'' and y_y'' are the modified orthogonal field components immediately after propagation through the half wave plate and q is the angle between the fast axis of the half wave plate and the plane of the incident polarisation. Hence, the field components, $y_x''(x_2, y_2)$ and $y_y''(x_2, y_2)$, immediately after the half wave plate are given by

$$\begin{aligned} y_x''(x_2, y_2) &= y_x'(x_2, y_2)\cos 2q + y_y'(x_2, y_2)\sin 2q \\ y_y''(x_2, y_2) &= -y_x'(x_2, y_2)\sin 2q + y_y'(x_2, y_2)\cos 2q \end{aligned} \tag{4.33}$$

where the symbols have their usual meaning. The orthogonal field components then propagate, without further modification, towards the polarising beamsplitter and differential photo-detector arrangement. The *x* field component propagates through the polarising beamsplitter and is incident on photo-detector 1, and the *y* field component is reflected at the beamsplitter interface and is incident on photo-detector 2. The signals from the two photo-detectors are calculated as previously and are given by the integral, over the surface of the photo-detector, of the square magnitude of the incident field distributions. Hence, the signals from the two photo-detectors are given by

$$I_{Det1}(x_s, y_s) = \iint_{-\infty}^{\infty} \left| y_x''(x_2, y_2) \right|^2 dx_2 dy_2$$
$$I_{Det2}(x_s, y_s) = \iint_{-\infty}^{\infty} \left| y_y''(x_2, y_2) \right|^2 dx_2 dy_2 \tag{4.34}$$

where it is assumed the photo-detectors are of equal responsivity, which is uniform and equal to unity over the surface of the photo-detectors.

The differential signal is found by subtracting the signals from the two photo-detectors and is given by

$$I(x_s, y_s) = I_{Det1}(x_s, y_s) - I_{Det2}(x_s, y_s) = \iint_{-\infty}^{\infty} \left| y_x''(x_2, y_2) \right|^2 - \left| y_y''(x_2, y_2) \right|^2 dx_2 dy_2 \tag{4.35}$$

which substituting for $y_x''(x_2, y_2)$ and $y_y''(x_2, y_2)$ from eq. (4.33) gives

$$I(x_s, y_s) = \iint_{-\infty}^{\infty} \left| y_x'(x_2, y_2)\cos 2q + y_y'(x_2, y_2)\sin 2q \right|^2 - \left| -y_x'(x_2, y_2)\sin 2q + y_y'(x_2, y_2)\cos 2q \right|^2 dx_2 dy_2 \tag{4.36}$$

Substituting for $y_x'(x_2, y_2)$ and $y_y'(x_2, y_2)$ from eq. (4.5) and rearranging gives

$$I(x_s, y_s) = \iint_{-\infty}^{\infty} \left| p_2(x_2, y_2) \right|^2 \left[\left| y_x(x_2, y_2)\cos 2q + y_y(x_2, y_2)\sin 2q \right|^2 - \left| -y_x(x_2, y_2)\sin 2q + y_y(x_2, y_2)\cos 2q \right|^2 \right] dx_2 dy_2 \tag{4.37}$$

where the symbols have their usual meaning. Substituting for $y_x(x_2, y_2)$ and $y_y(x_2, y_2)$ using eq. (4.4) and rearranging gives

$$I(x_s, y_s) = \iint \iint \left[\iint_{-\infty}^{\infty} \left| p_2(x_2, y_2) \right|^2 \exp\left\{ \frac{jk}{f} \left(x_2(x_o - x_o') + y_2(y_o - y_o') \right) \right\} dx_2 dy_2 \right]$$
$$\cdot \Big[\left(y_x'(x_o, y_o)\cos 2q + y_y'(x_o, y_o)\sin 2q \right) \left(y_x'^*(x_o', y_o')\cos 2q + y_y'^*(x_o', y_o')\sin 2q \right)$$
$$- \left(-y_x'(x_o, y_o)\sin 2q + y_y'(x_o, y_o)\cos 2q \right) \left(-y_x'^*(x_o', y_o')\sin 2q + y_y'^*(x_o', y_o')\cos 2q \right) \Big]$$
$$dx_2 dy_2 \tag{4.38}$$

which by substituting for $y_x'(x_o, y_o)$ and $y_y'(x_o, y_o)$ from eq. (4.3) and $g(x_o, y_o)$ from eq. (3.11) gives

$$
\begin{aligned}
I(x_s,y_s) = \iint\iint\ & g(x_o - x_o', y_o - y_o')h_1(x_o,y_o)h_1{}^*(x_o', y_o') \\
\cdot\Big[\ & \big(r_x(x_o - x_s, y_o - y_s)\cos 2q \\
& + r_x(x_o - x_s, y_o - y_s)\tan\big(a(x_o - x_s, y_o - y_s)\big)\exp\{-jf(x_o - x_s, y_o - y_s)\}\sin 2q\big) \\
& \cdot\big(r_x{}^*(x_o'-x_s, y_o'-y_s)\cos 2q \\
& + r_x{}^*(x_o'-x_s, y_o'-y_s)\big[\tan\big(a(x_o'-x_s, y_o'-y_s)\big)^*\big]\exp\{jf(x_o'-x_s, y_o'-y_s)\}\sin 2q\big) \\
& -\big(-r_x(x_o - x_s, y_o - y_s)\sin 2q \\
& + r_x(x_o - x_s, y_o - y_s)\tan\big(a(x_o - x_s, y_o - y_s)\big)\exp\{-jf(x_o - x_s, y_o - y_s)\}\cos 2q\big) \\
& \cdot\big(-r_x{}^*(x_o'-x_s, y_o'-y_s)\sin 2q \\
& + r_x{}^*(x_o'-x_s, y_o'-y_s)\big[\tan\big(a(x_o'-x_s, y_o'-y_s)\big)^*\big]\exp\{jf(x_o'-x_s, y_o'-y_s)\}\cos 2q\big)\ \Big] \\
& dx_o dy_o dx_o' dy_o'
\end{aligned}
\tag{4.39}
$$

which represents the signal from the Type 1 differential detector MO system for an arbitrary half wave plate fast axis angle $q°$.

The signal from the differential detector MO system is maximised when the angle subtended by the fast axis of the half wave plate and the angle of incident polarisation is $q = 22.5°$. The resultant signal from the Type 1 differential detector MO scanning microscope in this case is then

$$
\begin{aligned}
I(x_s,y_s) = \iint\iint\ & g(x_o - x_o', y_o - y_o')h_1(x_o,y_o)h_1{}^*(x_o', y_o') \\
\cdot\Big[\ & \big(r_x(x_o - x_s, y_o - y_s)r_x{}^*(x_o'-x_s, y_o'-y_s)\big[\tan\big(a(x_o'-x_s, y_o'-y_s)\big)^*\big]\exp\{jf(x_o'-x_s, y_o'-y_s)\} \\
& + \big(r_x{}^*(x_o'-x_s, y_o'-y_s)r_x(x_o - x_s, y_o - y_s)\tan\big(a(x_o - x_s, y_o - y_s)\big)\exp\{-jf(x_o - x_s, y_o - y_s)\}\big)\ \Big] \\
& dx_o dy_o dx_o' dy_o'
\end{aligned}
\tag{4.40}
$$

Transfer function representation

A transfer function representation of the signal generated in the Type 1 differential detector MO scanning microscope can be generated using the same analysis as was presented for the single detector MO system.

Expressing the reflectance and MO properties of the sample in terms of their associated spectra, $\Gamma(n_x,n_y)$ and $\Lambda(n_x,n_y)$ respectively as given by eq. (4.13), allows eq. (4.39) to be expressed in the form

$$
\begin{aligned}
I(x_s,y_s) = \iint_{-\infty}^{\infty}\iint & \left[\iint_{-\infty}^{\infty}\iint g(x_o - x_o', y_o - y_o') h_1(x_o,y_o) h_1^*(x_o',y_o') \right. \\
& \left. \cdot \exp\{-2pj(n_x x_o + n_y y_o)\} \exp\{2pj(n'_x x_o' + n_y' y_o')\} dx_o dy_o dx_o' dy_o' \right] \\
\cdot & \left[\left(\Gamma(n_x,n_y)\cos 2q + \Lambda(n_x,n_y)\sin 2q\right)\left(\Gamma^*(n_x',n_y')\cos 2q + \Lambda^*(n_x',n_y')\sin 2q\right) \right. \\
& \left. -\left(-\Gamma(n_x,n_y)\sin 2q + \Lambda(n_x,n_y)\cos 2q\right)\left(-\Gamma^*(n_x',n_y')\sin 2q + \Lambda^*(n_x',n_y')\cos 2q\right) \right] \\
& dn_x dn_y dn_x' dn_y'
\end{aligned}
\tag{4.41}
$$

which by comparison with eq. (3.31) can be further simplified to give the characteristic equation expressed in eq. (3.32), i.e.

$$
\begin{aligned}
I(x_s,y_s) = \iint_{-\infty}^{\infty}\iint & C(n_x,n_y;n_x',n_y') M(n_x,n_y;n_x',n_y') \\
& \cdot \exp\{2p\, j[(n_x - n_x')x_s + (n_y - n_y')y_s]\}\ dn_x\, dn_y\, dn_x'\, dn_y'
\end{aligned}
\tag{3.32}
$$

where $C(n_x,n_y;n_x',n_y')$ represents the Type 1 PCTF. However, in the differential detector MO scanning microscope the medium function, $M(n_x,n_y;n_x',n_y')$, is now given by

$$
\begin{aligned}
M(n_x,n_y;n_x',n_y') = & \left(\Gamma(n_x,n_y)\Gamma^*(n_x',n_y') - \Lambda(n_x,n_y)\Lambda^*(n_x',n_y')\right)\cos 4q \\
& + \left(\Gamma(n_x,n_y)\Lambda^*(n_x,n_y) + \Gamma^*(n_x',n_y')\Lambda(n_x,n_y)\right)\sin 4q
\end{aligned}
\tag{4.42}
$$

where the symbols have their usual meaning.

If the half wave plate is aligned so as to maximise the Kerr signal from the differential amplifier, i.e. $q = 22.5°$, then the medium function reduces to

$$M\left(n_x, n_y; n_x', n_y'\right) = \left(\Gamma\left(n_x, n_y\right)\Lambda^*\left(n_x, n_y\right) + \Gamma^*\left(n_x', n_y'\right)\Lambda\left(n_x, n_y\right)\right) \quad . \quad (4.43)$$

The response of the Type 1 differential detector MO scanning microscope can now be modelled in computer code using the 'direct calculation' approach for simple one-dimensional and two-dimensional MO objects, which is described in sec. 5.3, and the 'transfer function' approach for simple one-dimensional objects, which is described in sec. 6.4.1.

4.2.2 The confocal system

It has already been mentioned that the confocal arrangement of the differential detector MO scanning microscope is often used by researchers to study magnetic thin films. Hence, it is useful to investigate the readout mechanism in such an imaging system and to compare its imaging characteristics with those of the Type 1 configuration.

Optical configuration

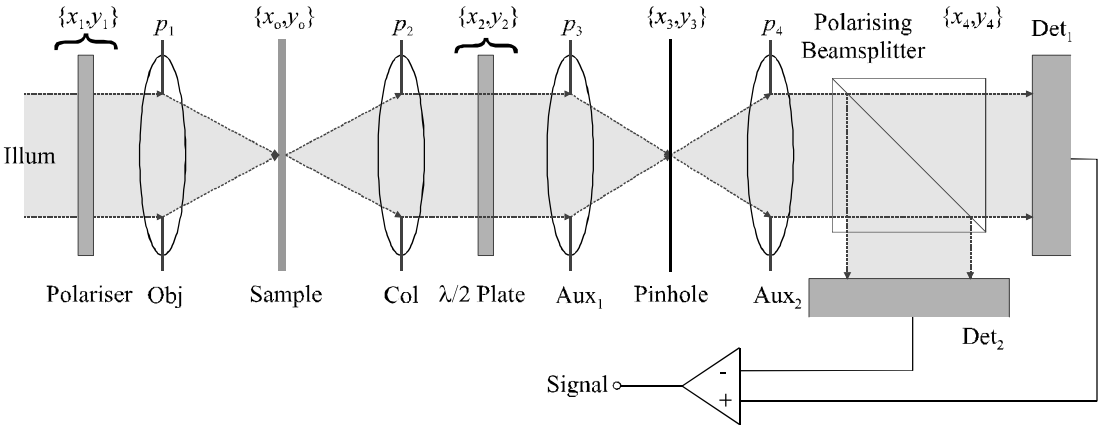

Figure 4.4 : *The optical layout of the confocal differential detector MO scanning microscope.*

Figure 4.4 illustrates the optical channel of the confocal arrangement of the differential detector MO scanning microscope.

The pinhole aperture and auxiliary lens arrangement is introduced between the half wave plate and the polarising beamsplitter and differential detector arrangement.

Image calculation

The orthogonal field distributions immediately after propagation through the half wave plate are as given in the Type 1 differential detector MO system, eq. (4.33).

The orthogonal polarised field components, $y_x'''(x_2, y_2)$ and $y_y'''(x_2, y_2)$, immediately after propagating through auxiliary lens 1 are given by

$$\begin{aligned} y_x'''(x_2, y_2) &= p_3(x_2, y_2) y_x''(x_2, y_2) \\ &= p_3(x_2, y_2)\left(y_x'(x_2, y_2)\cos 2q + y_y'(x_2, y_2)\sin 2q\right) \\ y_y'''(x_2, y_2) &= p_3(x_2, y_2) y_y''(x_2, y_2) \\ &= p_3(x_2, y_2)\left(-y_x'(x_2, y_2)\sin 2q + y_y'(x_2, y_2)\cos 2q\right) \end{aligned} \tag{4.44}$$

where $p_3(x_2, y_2)$ is the aperture pupil function of auxiliary lens 1 and all other symbols have their usual meaning. The orthogonal field components, $y_x(x_3, y_3)$ and $y_y(x_3, y_3)$, in the plane of the confocal pinhole are given by the two-dimensional Fourier transform of the field components, $y_x'''(x_2, y_2)$ and $y_y'''(x_2, y_2)$, immediately after auxiliary lens 1, i.e.

$$\begin{aligned} y_x(x_3, y_3) &= \frac{1}{l f_{A1}} \iint_{-\infty}^{\infty} y_x'''(x_2, y_2) \exp\left\{\frac{jk}{f_{A1}}(x_3 x_2 + y_3 y_2)\right\} dx_2 dy_2 \\ y_y(x_3, y_3) &= \frac{1}{l f_{A1}} \iint_{-\infty}^{\infty} y_y'''(x_2, y_2) \exp\left\{\frac{jk}{f_{A1}}(x_3 x_2 + y_3 y_2)\right\} dx_2 dy_2 \end{aligned} \tag{4.45}$$

where f_{A1} is the focal length of auxiliary lens 1. The orthogonal field distributions are modified by the aperture pupil function of the confocal pinhole, $p_p(x_3, y_3)$, to give

$$\begin{aligned} y_x'(x_3, y_3) &= p_p(x_3, y_3) y_x(x_3, y_3) \\ y_y'(x_3, y_3) &= p_p(x_3, y_3) y_y(x_3, y_3) \end{aligned} \quad . \tag{4.46}$$

The orthogonal field distributions, $y_x(x_4, y_4)$ and $y_x(x_4, y_4)$,in the plane of auxiliary lens 2 are given by the two-dimensional Fourier transform of the field distributions, $y_x'(x_3, y_3)$ and $y_y'(x_3, y_3)$, immediately after the pinhole aperture, i.e.

$$\begin{aligned} y_x(x_4, y_4) &= \frac{1}{lf_{A2}} \iint_{-\infty}^{\infty} y_x'(x_3, y_3) \exp\left\{ \frac{jk}{f_{A2}} (x_4 x_3 + y_4 y_3) \right\} dx_3 dy_3 \\ y_y(x_4, y_4) &= \frac{1}{lf_{A2}} \iint_{-\infty}^{\infty} y_y'(x_3, y_3) \exp\left\{ \frac{jk}{f_{A2}} (x_3 x_4 + y_4 y_3) \right\} dx_3 dy_3 \end{aligned} \tag{4.47}$$

where f_{A2} is the focal length of auxiliary lens 2. These field distributions are modified by the aperture pupil function of auxiliary lens 2, $p_4(x_4, y_4)$, to give

$$\begin{aligned} y_x'(x_4, y_3) &= p_4(x_4, y_4) y_x(x_4, y_4) \\ y_y'(x_4, y_4) &= p_4(x_4, y_4) y_y(x_4, y_4) \end{aligned} \quad . \tag{4.48}$$

The orthogonal field components then propagate, without further modification, towards the polarising beamsplitter and differential photo-detector arrangement. Assuming that the *x* field component propagates through the polarising beamsplitter towards photo-detector 1, and that the *y* field component is reflected at the polarising beamsplitter interface towards photo-detector 2, then the signal from the confocal differential detector MO system is given by

$$I(x_s, y_s) = I_{Det1}(x_s, y_s) - I_{Det2}(x_s, y_s) = \iint_{-\infty}^{\infty} \left| y_x'(x_4, y_4) \right|^2 - \left| y_y'(x_4, y_4) \right|^2 dx_4 dy_4 \tag{4.49}$$

where it is assumed that the photo-detectors are of equal, uniform responsivity (set to unity). Substituting for $y_x'(x_4, y_4)$ and $y_y'(x_4, y_4)$ from eq. (4.48), and rearranging gives

$$I(x_s, y_s) = \iint_{-\infty}^{\infty} \left| p_4(x_4, y_4) \right|^2 \left(\left| y_x(x_4, y_4) \right|^2 - \left| y_y(x_4, y_4) \right|^2 \right) dx_4 dy_4 \quad . \tag{4.50}$$

Again, assuming that auxiliary lens 2 collects all the field emanating from the pinhole, then $p_4(x_4, y_4)$ can be set to unity and eq. (4.50) simplifies to

$$I(x_s, y_s) = \iint_{-\infty}^{\infty} \left| p_p(x_3, y_3) \right|^2 \left(\left| y_x(x_3, y_3) \right|^2 - \left| y_y(x_3, y_3) \right|^2 \right) dx_3 dy_3 \quad . \tag{4.51}$$

Substituting for $y_x(x_3, y_3)$ and $y_y(x_3, y_3)$ from eq. (4.45), and rearranging gives

$$I(x_s,y_s)=\iint_{-\infty}^{\infty}\iint_{-\infty}^{\infty}\left[\iint_{-\infty}^{\infty}\left|p_p(x_3,y_3)\right|^2\exp\left\{\frac{jk}{f_{A1}}\left(x_3(x_2-x_2')+y_3(y_2-y_2')\right)\right\}dx_3dy_3\right]$$
$$\cdot\left(y_x'''(x_2,y_2)y_x'''^*(x_2',y_2')-y_y'''(x_2,y_2)y_y'''^*(x_2',y_2')\right)dx_2dy_2dx_2'dy_2' \tag{4.52}$$

which simplifies to

$$I(x_s,y_s)=\iint_{-\infty}^{\infty}\iint_{-\infty}^{\infty}G(x_2-x_2',y_2-y_2')$$
$$\cdot\left(y_x'''(x_2,y_2)y_x'''^*(x_2',y_2')-y_y'''(x_2,y_2)y_y'''^*(x_2',y_2')\right)dx_2dy_2dx_2'dy_2' \tag{4.53}$$

where $G(x_2,y_2)$ is the Fourier transform of the square magnitude of the pinhole aperture pupil function and is given by eq. (3.62). Substituting for $y_x'''(x_2,y_2)$ and $y_y'''(x_2,y_2)$ from eq. (4.44) and rearranging gives

$$I(x_s,y_s)=\iint_{-\infty}^{\infty}\iint_{-\infty}^{\infty}G(x_2-x_2',y_2-y_2')p_c(x_2,y_2)p_c^*(x_2',y_2')$$
$$\cdot\Big[\left(y_x(x_2,y_2)\cos 2q+y_y(x_2,y_2)\sin 2q\right)\left(y_x^*(x_2',y_2')\cos 2q+y_y^*(x_2',y_2')\sin 2q\right)$$
$$-\left(-y_x(x_2,y_2)\sin 2q+y_y(x_2,y_2)\cos 2q\right)\left(-y_x^*(x_2',y_2')\sin 2q+y_y^*(x_2',y_2')\cos 2q\right)\Big]$$
$$dx_2dy_2dx_2'dy_2' \tag{4.54}$$

Substituting for $y_x(x_2,y_2)$ and $y_y(x_2,y_2)$ from eq. (4.4) and rearranging gives

$$I(x_s,y_s)=\iint_{-\infty}^{\infty}\iint_{-\infty}^{\infty}\Big[\iint_{-\infty}^{\infty}\iint_{-\infty}^{\infty}G(x_2-x_2',y_2-y_2')p_c(x_2,y_2)p_c^*(x_2',y_2')$$
$$\cdot\exp\left\{\frac{jk}{f}\left(x_2x_o-y_2y_o\right)\right\}\exp\left\{\frac{-jk}{f}\left(x_2'x_o'-y_2'y_o'\right)\right\}dx_2dy_2dx_2'dy_2'\Big]$$
$$\cdot\Big[\left(y_x'(x_o,y_o)\cos 2q+y_y'(x_o,y_o)\sin 2q\right)\left(y_x'^*(x_o',y_o')\cos 2q+y_y'^*(x_o',y_o')\sin 2q\right)$$
$$-\left(-y_x'(x_o,y_o)\sin 2q+y_y'(x_o,y_o)\cos 2q\right)\left(y_x'^*(x_o',y_o')\sin 2q+y_y'^*(x_o',y_o')\cos 2q\right)\Big]$$
$$dx_ody_odx_o'dy_o' \tag{4.55}$$

which simplifies to

$$I(x_s,y_s)=\iint_{-\infty}^{\infty}\iint g(x_o,y_o;x_o',y_o')$$
$$\Big[\Big(\cos 2q\,y_x'(x_o,y_o)+\sin 2q\,y_y'(x_o,y_o)\Big)\Big(y_x'^*(x_o',y_o')\cos 2q+y_y'^*(x_o',y_o')\Big)\sin 2q$$
$$-\Big(-y_x'(x_o,y_o)\sin 2q+y_y'(x_o,y_o)\cos 2q\Big)\Big(-y_x'^*(x_o',y_o')\sin 2q+y_y'^*(x_o',y_o')\cos 2q\Big)\Big] \tag{4.56}$$
$$dx_o\,dy_o\,dx_o'\,dy_o'$$

where $g(x_o,y_o;x_o',y_o')$ is given by eq. (3.49). Finally, substituting for $y_x'(x_o,y_o)$ and $y_y'(x_o,y_o)$ from eq. (4.3) and rearranging gives

$$I(x_s,y_s)=\iint\iint g(x_o,y_o;x_o',y_o')h_1(x_o,y_o)h_1^*(x_o',y_o')\Big[\Big(r_x(x_o-x_s,y_o-y_s)\cos 2q$$
$$+r_x(x_o-x_s,y_o-y_s)\tan\big(a(x_o-x_s,y_o-y_s)\big)\exp\{-jf(x_o-x_s,y_o-y_s)\}\sin 2q\Big)$$
$$\cdot\Big(r_x^*(x_o'-x_s,y_o'-y_s)\cos 2q$$
$$+r_x^*(x_o'-x_s,y_o'-y_s)\big[\tan\big(a(x_o'-x_s,y_o'-y_s)\big)^*\big]\exp\{jf(x_o'-x_s,y_o'-y_s)\}\sin 2q\Big)$$
$$-\Big(-r_x(x_o-x_s,y_o-y_s)\sin 2q$$
$$+r_x(x_o-x_s,y_o-y_s)\tan\big(a(x_o-x_s,y_o-y_s)\big)\exp\{-jf(x_o-x_s,y_o-y_s)\}\cos 2q\Big)$$
$$\cdot\Big(-r_x^*(x_o'-x_s,y_o'-y_s)\sin 2q$$
$$+r_x^*(x_o'-x_s,y_o'-y_s)\big[\tan\big(a(x_o'-x_s,y_o'-y_s)\big)^*\big]\exp\{jf(x_o'-x_s,y_o'-y_s)\}\cos 2q\Big)\Big]dx_o\,dy_o\,dx_o'\,dy_o' \tag{4.57}$$

which represents the signal from the confocal differential detector MO scanning microscope for an arbitrary half wave plate angle $q°$.

Transfer function representation

A transfer function representation of the signal from the confocal differential detector MO scanning microscope can be generated using the same procedure as was presented for the previous MO scanning microscopes.

Expressing the reflectance and MO properties of the sample in terms of their associated spectra, $\Gamma(n_x,n_y)$ and $\Lambda(n_x,n_y)$ respectively as given by eq. (4.13), allows eq. (4.40) to be expressed in the form

$$I(x_s, y_s) = \iint_{-\infty}^{\infty}\iint \left[\iint_{-\infty}^{\infty}\iint g(x_o, y_o; x_o', y_o') h_1(x_o, y_o) h_1^*(x_o', y_o') \right.$$
$$\left. \cdot \exp\{-2pj(n_x x_o + n_y y_o)\} \exp\{2pj(n'_x x_o' + n_y' y_o')\} dx_o dy_o dx_o' dy_o' \right]$$
$$\cdot \left[\left(\Gamma(n_x, n_y)\cos 2q + \Lambda(n_x, n_y)\sin 2q\right)\left(\Gamma^*(n_x', n_y')\cos 2q + \Lambda^*(n_x', n_y')\sin 2q\right) \right.$$
$$\left. -\left(-\Gamma(n_x, n_y)\sin 2q + \Lambda(n_x, n_y)\cos 2q\right)\left(-\Gamma^*(n_x', n_y')\sin 2q + \Lambda^*(n_x', n_y')\cos 2q\right) \right]$$
$$dn_x dn_y dn_x' dn_y' \qquad (4.58)$$

where the symbols have their usual meaning. Comparing eq. (4.58) with eq. (4.41) it can be seen that the signal from the confocal differential detector configuration can be expressed in the characteristic form of eq. (3.32), where the medium function is as for the Type 1 differential detector MO scanning microscope, eq. (4.42) and the PCTF is now given by the confocal PCTF of eq. (3.73).

In sec. 6.4.2 the transfer function approach will be used to model the response of the confocal differential detector MO scanning microscope for simple one-dimensional MO objects.